Single-Shot Spin Readout in Graphene Quantum Dots

Lisa Maria Gächter,[1,*,‡] Rebekka Garreis,[1,†,‡] Jonas Daniel Gerber,[1] Max Josef Ruckriegel,[1] Chuyao Tong,[1] Benedikt Kratochwil,[1] Folkert Kornelis de Vries,[1] Annika Kurzmann,[1] Kenji Watanabe,[2] Takashi Taniguchi,[2] Thomas Ihn,[1] Klaus Ensslin,[1] and Wister Wei Huang[1]

[1] *Solid State Physics Laboratory, ETH Zurich, Zurich CH-8093, Switzerland*

[2] *National Institute for Material Science, 1-1 Namiki, Tsukuba 305-0044, Japan*

(Received 21 December 2021; revised 11 March 2022; accepted 15 April 2022; published 26 May 2022)

Electrostatically defined quantum dots in bilayer graphene offer a promising platform for spin qubits with presumably long coherence times due to low spin-orbit coupling and low nuclear spin density. We demonstrate two different experimental approaches to measure the decay times of excited states. The first is based on direct current measurements through the quantum device. Pulse sequences are applied to control the occupation of ground and excited states. We observe a lower bound for the excited state decay on the order of a hundred microseconds. The second approach employs a capacitively coupled charge sensor to study the time dynamics of the excited state using the Elzerman technique. We perform single-shot readout of our two-level system with a signal-to-noise ratio of about 7 and find relaxation times up to 50 ms for the spin-excited state, with a strong magnetic field dependence, promising even higher values for smaller magnetic fields. This is an important step for developing a quantum-information processor in graphene.

DOI: 10.1103/PRXQuantum.3.020343

I. INTRODUCTION

Spin qubits in semiconductors [1,2] have the advantage that the operation and fabrication of gate electrodes are similar to classical transistors. High-quality qubits have been demonstrated on traditional bulk MOSFETs [3–5] as well as on III-V [6–8], silicon- [9–12] and germanium- [13] based heterostructures. Furthermore, semi-industrial structures compatible with industrial Si technologies, such as fully depleted silicon-on-insulator (FD SOI) transistors [14] and fin field-effect transistors (FinFETs) [15], have been investigated.

Graphene offers several advantages as a host material for spin qubits, namely naturally low nuclear spin concentrations and weak spin-orbit interactions, similar to Si. In addition, the two-dimensional nature of graphene allows for much smaller and possibly more strongly coupled quantum devices [16]. Furthermore, bilayer graphene quantum dots (QDs) offer the flexibility of bipolar operation [17]. Compared to the mature Si-based technology, the development of quantum devices in graphene is in its infancy. Recent advances in the controllability of individual states in single QDs [17–20] and double QDs [21,22], as well as the implementation of charge detection [23], enable the realization of spin qubits based on electrostatically defined QDs in bilayer graphene. Major milestones such as qubit manipulation and detection have yet to be achieved to unlock the qubit potential of graphene.

Single-shot readout is an essential first step towards building a universal quantum computer and implementing quantum algorithms and quantum error detection. In order to reach the single-shot readout limit, it is critical for the excited-state relaxation time to be longer than the measurement time to resolve a single charge tunneling event. We first investigate the relaxation time by measuring the current flowing through a QD [24,25], which allows us to extract a lower bound only, similar to previous experiments [26]. In order to study the time dynamics of the excited state beyond the microsecond regime, we add a charge detector to the device design and perform time-resolved measurements of the tunneling events in the QD. This allows us to perform single-shot readout of the two-level system using the Elzerman technique [27]. We measure spin-relaxation times up to 50 ms at $B_\perp = 1.7$ T. We find a strong dependence of T_1 on the external magnetic field, promising even higher values for smaller spin splitting. The spin-relaxation time presented in this paper is a few orders of magnitude longer than typical spin-qubit operation times [28,29] and competes very well with other group-IV elements, like silicon [30,31].

*lisag@phys.ethz.ch

†garreisr@phys.ethz.ch

‡These authors contributed equally to this paper.

II. PULSED-GATE SPECTROSCOPY

A false-color atomic force micrograph of the device is shown in Fig. 1(a). It consists of a *h*-BN encapsulated bilayer graphene flake on top of a global graphite back gate with gold electrodes patterned on top. The gate layers are separated by 30-nm atomic-layer-deposited aluminium oxide [17]. We form an *n*-type channel connecting source and drain by operating the back gate at $V_{\mathrm{BG}} = 5$ V and the split gates at $V_{\mathrm{SG}} = -3.13$ V. Three finger gates are used to control the potential locally along the channel [see Fig. 1(a)]. The outer two finger gates TL and TR act as tunable tunnel barriers separating the QD from the left and right reservoirs. With increasingly negative voltage applied to the middle finger gate (the plunger gate), we locally lower the Fermi energy set by the back gate, subsequently loading holes into the QD forming below the gate. The sample is mounted in a dilution refrigerator with a base temperature of 9 mK on a printed circuit board equipped with low-pass-filtered dc lines and 50-Ω impedance matched ac lines to perform pulsed-gate experiments. The plunger gate is connected to a bias tee allowing for dc and ac control [e.g., applying a pulse as sketched in Fig. 1(b)] while all other gates and the Ohmic contacts are connected to dc lines only.

We first define our two-level system. Due to spin and valley degrees of freedom in bilayer graphene, the single-particle orbital states are fourfold degenerate, with two spins ($\uparrow, \downarrow$) and two valleys (K and K') [18,32]. A perpendicular magnetic field, $B_\perp$, lifts the degeneracy due to the spin (s) and valley (v) Zeeman effect following $E(B_\perp) = \pm(1/2) g_{s,v} \mu_B B_\perp$, with the spin g factor g_s, the valley g factor g_v, and the Bohr magneton μ_B. Typical values around $g_v = 30$ [17] ensure that at electron temperatures below 100 mK, the two lowest energy levels are valley polarized already at perpendicular magnetic fields $B_\perp > 50$ mT. As we operate our device at much higher fields, above $B_\perp = 1.75$ T, we can consider our QD as an effective two-level spin system with the ground state (GS) $|K' \uparrow\rangle$ and the excited state (ES) $|K' \downarrow\rangle$ energetically split by $\Delta E = \Delta_{\mathrm{SO}} + g_s \mu_B B$ with the zero-field spin-orbit splitting Δ_{SO} with typical values on the order of 60 μeV [20–22,33,34].

To experimentally access the single-particle spectrum we perform finite-bias spectroscopy measurements around the $N = 0$ to $N = 1$ hole transition at $B_\perp = 1.75$ T [Fig. 1(c)]. The two lowest K'-polarized energy states $|K' \uparrow\rangle$ and $|K' \downarrow\rangle$, from now on denoted as $|\downarrow\rangle$ and $|\uparrow\rangle$ for ease of notation, are well observable while the K states are split off and would only become visible for a larger bias window.

To confirm the nature of the ES we apply an additional in-plane magnetic field $B_\parallel$, which couples only to the spin degree of freedom. Keeping the perpendicular magnetic field $B_\perp = 1.75$ T and the plunger gate voltage V_{PG} fixed

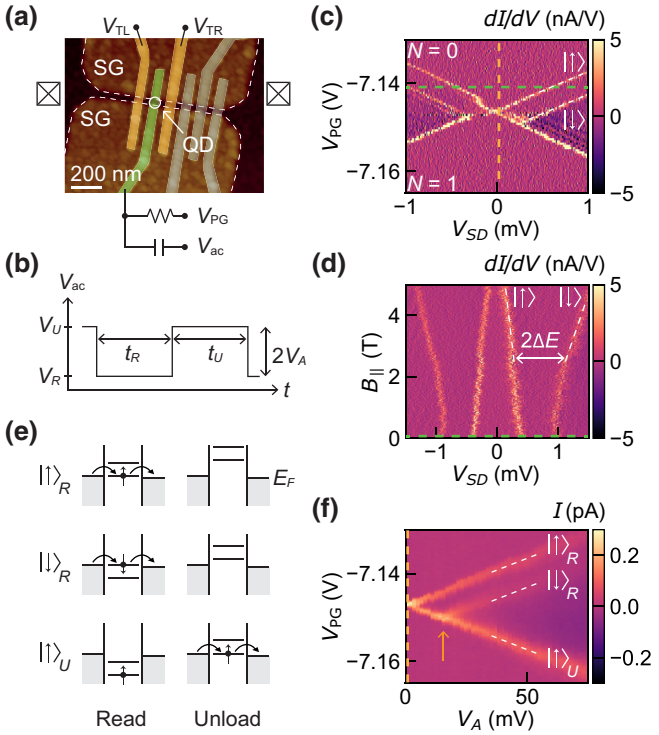

FIG. 1. (a) False-color micrograph of the device. The plunger gate (green) is controlled with dc voltage (V_{PG}) and ac pulses (V_{ac}) combined by a bias tee. The black squares with crosses inside symbolize Ohmic contacts. (b) The ac pulse sequence consists of a read phase with pulse level $V_R = -V_A$ and duration t_R and an unload phase with pulse level $V_U = V_A$ and duration t_U. (c) Coulomb diamond of the first hole transition taken at $B_\perp = 1.75$ T. For large source-drain voltage V_{SD} the excited-state resonance can be observed. (d) In-plane magnetic field dependence at fixed plunger gate voltage, corresponding to green horizontal dashed line in (c). The splitting of the GS and the ES at high magnetic field is consistent with a spin g factor of 2. (e) Schematic of transport through $|\uparrow\rangle_R$ and $|\downarrow\rangle_R$ during read phase and through $|\uparrow\rangle_U$ during unload phase. For ease of understanding an electronlike level scheme is used, while hole states are probed in the experiment. (f) Coulomb resonance as a function of pulse amplitude at pulse frequency $f = 1.25$ MHz. $V_A = 0$ V corresponds to a line cut along the orange vertical dashed line in (c) at $V_{SD} = 40$ μeV. For finite pulse amplitudes V_A, the transition $|\uparrow\rangle$ splits into two branches, $|\uparrow\rangle_R$ and $|\uparrow\rangle_U$, due to the two-level pulsing. For pulse amplitudes $e\alpha_{\mathrm{att}}\alpha_{\mathrm{PG}}V_A > E_Z$, see orange arrow, transport through the ES is allowed by the pulse during the read phase and shows up as $|\downarrow\rangle_R$ in between the GS peaks.

[horizontal dashed line in Fig. 1(c)] we perform finite-bias spectroscopy measurements, varying the in-plane magnetic field $B_\parallel$ [Fig. 1(d)]. The splitting ΔE as a function of magnetic field corresponds to a g factor of 2 and a zero-field spin-orbit splitting $\Delta_{\mathrm{SO}} \approx 60$ μeV, consistent with a spin ES.

We then perform transient current spectroscopy measurements at a source-drain voltage $V_{SD} = 40$ μV $\ll k_B T$

to study the relaxation of the ES to the GS. We apply an ac pulse additional to the dc voltage on the plunger gate, effectively shifting the QD states with respect to the Fermi level of the reservoirs in time. We start with two-level pulses each consisting of a read and an unload phase as shown in Fig. 1(b) with corresponding voltages V_R and V_U and pulse widths t_R and t_U. During t_U, both $|\uparrow\rangle$ and $|\downarrow\rangle$ are pulsed above the Fermi level E_F of the leads and the QD is emptied. During t_R, if $|\uparrow\rangle$ is aligned with E_F we observe a steady current. If $|\downarrow\rangle$ is aligned with E_F during t_R while $|\uparrow\rangle$ lies below, holes can only tunnel through the QD ES until one of them relaxes with a spin flip or until direct tunneling from the leads into the GS occurs. This effectively blocks transport until the QD gets emptied again in the subsequent unload phase. Figure 1(f) shows the current through the QD as a function of pulse amplitude V_A and V_{PG} for $t_U = t_R = 400$ ns. We observe the splitting of the Coulomb resonance into two peaks, corresponding to transient current through the GS of the read level, $|\uparrow\rangle_R$, and the unload level, $|\uparrow\rangle_U$. At $2V_A = 100$ mV, the peaks are separated by $\Delta V_{\mathrm{PG}} = 21$ mV. This splitting is consistent with the 13-dB attenuation installed along the high-frequency line of our setup. The slope of the GS splitting, together with the plunger gate lever arm, give us the conversion factor from pulse amplitude to energy scale $\alpha_{\mathrm{att}}\alpha_{\mathrm{PG}}$, where $\alpha_{\mathrm{att}} = 0.21$ and $\alpha_{\mathrm{PG}} = 0.05$. For pulse amplitudes larger than the Zeeman splitting [indicated in Fig. 1(f)] the current peak corresponding to a transient current through the ES of the read level, $|\downarrow\rangle_R$, becomes visible as well. We observe the $|\downarrow\rangle_R$ peak, because a sufficiently high perpendicular magnetic field $B_\perp$ is applied. This not only lifts spin and valley degeneracies but also reduces the tunneling rates between the QD and the reservoirs. At low perpendicular magnetic field $|\downarrow\rangle_R$ is not visible, as the reduction of tunneling rates solely by voltages applied to the tunnel barrier gates TL and TR is not sufficient in this device (see Ref. [23]).

The longer the QD stays in the read phase, the more likely the hole relaxes into the GS $|\uparrow\rangle$. Therefore, studying the dependence of the amplitude of $|\downarrow\rangle_R$ on the pulse width t_R allows us to extract information about the relaxation time. However, two-level pulsed-gate spectroscopy only allows one to extract a lower bound for T_1, as this measurement scheme cannot distinguish between relaxation and direct tunneling into the GS during the read phase. Already Ref. [35] suffered from this limitation, stating a lower bound of $T_1 = 500$ ns. To improve on this limitation, we extend the pulsing sequence to four-level pulses with added load and wait phases in which both $|\uparrow\rangle$ and $|\downarrow\rangle$ are pulsed below the bias window [26,36]. The voltage and time for the load phase is chosen such that the time integral over voltages in one pulse sequence is zero, in order to avoid charging up the bias tee. The corresponding four-level pulse scheme is depicted in Fig. 2(a) with pulse widths $t_L = t_R = t_U = 1$ μs, and $t_W = 400$ ns and voltages

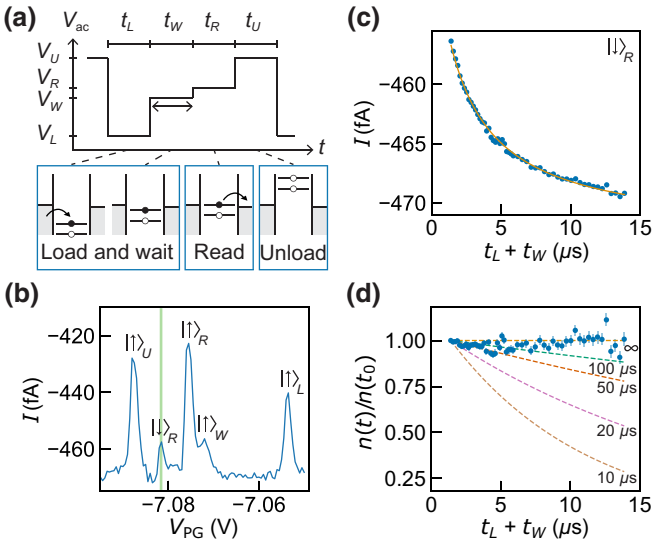

FIG. 2. (a) Four-level pulse scheme for relaxation-time measurements. The hole enters a random state during the load phase. If the hole is loaded into the GS it will stay there and no transport current can flow. If the carrier is loaded into the ES and does not relax during $t_L + t_W$, the charge carrier can tunnel out, resulting in a transport current in the read phase. The QD is then emptied in the unload phase and the cycle is repeated. (b) Current as a function of plunger gate voltage while applying the four-level pulse. We observe various peaks corresponding to GS and ES levels of different pulse phases being aligned with the bias window. This measurement is taken in a second cooldown at a $B_\perp = 1.9$ T, leading to a slight shift of V_{PG}. (c) Current corresponding to ES transport during the read phase [shaded in green in (b)] as a function of loading and waiting time. We vary the waiting time while the loading time remains constant at $t_L = 1$ μs. The decay results from a combination of lower cycling rate and ES relaxation time. As described in the main text the decay is dominated by signal decay. (d) Normalized average number of charge carriers per pulse cycle. Dashed color lines represent the decays with the corresponding relaxation time. Our result indicates that relaxation does not play a significant role during the measurement window.

$V_L = -9$ mV, $V_W = 0$ V, $V_R = 1.5$ mV, and $V_U = 7.5$ mV for the respective pulse periods. During the load and the wait phases both $|\uparrow\rangle$ and $|\downarrow\rangle$ levels are below the bias window, allowing a hole to tunnel into either one of the two states. During t_R, the ES $|\downarrow\rangle$ is aligned with the Fermi level of the leads while the GS $|\uparrow\rangle$ is still below, allowing for spin-selective tunneling.

Applying the four-level pulsing scheme while sweeping the dc plunger gate voltage V_{PG} results in a current trace as shown in Fig. 2(b). Assigning the observed current peaks to GS and ES levels being aligned with the bias window during various pulse phases, we identify the peak $|\downarrow\rangle_R$ (shaded in green), originating from holes tunneling through the ES from source to drain during the read phase. If it relaxes to $|\uparrow\rangle$ before the readout, it does not contribute to this current as it cannot tunnel out of the QD, making the

amplitude of the current peak a measure of the relaxation. Therefore, we investigate the amplitude of the current peak, $|\downarrow\rangle_R$, as a function of the waiting time $t_L + t_W$ as shown in Fig. 2(c). Increasing the waiting time inevitably decreases the ratio between the time spent in the read phase and the total pulse cycle time t_{total} causing signal decay in addition to relaxation. We find that the current can be fitted to [36] $I = \langle n\rangle e^{-(t_L+t_W)/T_1}/t_{\text{total}} + I_{\text{bg}}$ in the limit $T_1 \to \infty$, and therefore effectively to $I = \langle n\rangle/t_{\text{total}} + I_{\text{bg}}$ with high confidence. In these expressions, $\langle n\rangle$ is the average number of charge carriers per pulse cycle, t_{total} is the total duration of the four-level pulse, and I_{bg} is the background current level. This implies that, within our measurement time window the decay of the measured current through $|\downarrow\rangle_R$ is dominated by the signal strength reducing as the pulse cycle time t_{total} becomes longer for increasing t_W. Multiplying $(I - I_{\text{bg}})$ with the total time $t_L + t_W$ the GS and the ES levels are pulsed below E_F, we find the normalized probability $\langle n(t)\rangle/\langle n(t_0)\rangle = e^{-(t_L+t_W)/T_1}$ of the hole still being in the ES after the load and wait phase as a function of loading and waiting time, $t_L + t_W$, shown in Fig. 2(d). Based on this we conservatively estimate a lower bound for the relaxation time $T_1 \geq 100\ \mu$s. The data is acquired over 8 h over which the background current fluctuation can be larger than 0.1 fA and leads to an uncertainty in the offset current. Careful determination of I_{bg} is crucial as it affects the slope in Fig. 2(d). Further extending the waiting time inevitably leads to vanishingly small current beyond the detection limit of transport measurements. To overcome the signal strength limit, a more advanced readout mechanism is required.

III. SINGLE-SHOT SPIN DETECTION

Recent progress in fabrication techniques enabled the realization of a fully electrostatically defined device with an integrated charge detector as described in Ref. [23]. The device shown in Fig. 3(a) consists of two channels separated by a depletion region underneath a 150-nm-wide middle gate. Similar to the sample presented above we define a QD between two tunnel barriers (TL and TR) and use a plunger gate (PG) to tune the QD to single-electron occupation in channel 2. The charge detector is based on a second QD formed below a single finger gate (FG) in the current biased channel 1. A charge carrier tunneling on or off the QD in channel 2 changes the electrostatic potential in its surroundings, therefore also in the nearby sensing QD in channel 1. This potential change shifts the Coulomb resonances in the sensing QD and leads to a steplike change in the voltage across channel 1 [see middle panel of Fig. 3(d)], if the sensing QD is tuned to the steep slope of a conductance resonance. This sample is measured in a dilution refrigerator with an electron temperature of 45 mK, and the ac and dc signals are combined via two resistors as a voltage divider.

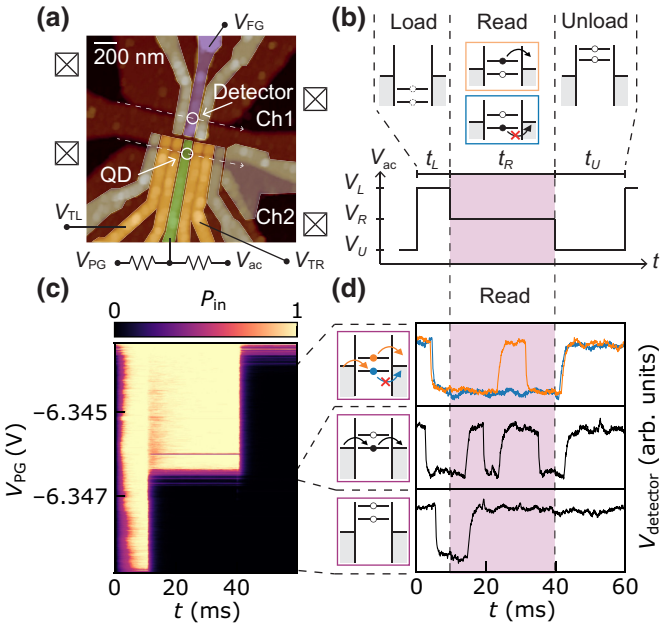

FIG. 3. (a) False-color micrograph of a single QD device with a nearby charge detector. The QD is formed beneath the plunger gate (green) in channel 2. TL and TR serve as tunnel barriers (yellow) to the leads. Another QD is formed under one finger gate (purple) in channel 1 and used as a charge detector. The black squares with crosses inside symbolize Ohmic contacts. (b) Three-level pulse scheme applied to the plunger gate. (c) Probability of the QD being occupied as a function of time and plunger gate dc voltage V_{PG} extracted from 500 single-shot traces. (d) Exemplary traces for different read levels. Top: ideal read-level configuration allowing for single-shot ES-selective readout. Middle: GS level is aligned with E_F corresponding to multiple tunneling events. Bottom: both the ES and GS level are pushed above E_F during the read phase, which results in a single tunneling-out event.

At a perpendicular magnetic field of 2.1 T, we find a spin ES split from the GS of the one-electron quantum dot by about 315 μeV [see Fig. S1(a) within the Supplemental Material [37]]. Extracting the energetic splitting of the ES $|\downarrow\rangle$ from the GS $|\uparrow\rangle$ for different magnetic fields yields a spin g factor of 2 and a spin-orbit coupling of $\Delta_{\text{SO}} \approx 70\ \mu$eV as presented in Fig. S1(b) within the Supplemental Material [37], which is consistent with previous results [20–22].

For the single-shot charge-detection experiment, we follow the scheme introduced by Elzerman in Ref. [27]. Figure 3(b) shows the voltage pulses applied to the plunger gate PG. Again, in the load phase either $|\uparrow\rangle$ or $|\downarrow\rangle$ can be loaded as both energy levels reside below the Fermi energy E_F of the leads. During the loading time t_L the charge carrier is trapped on the QD and Coulomb blockade prevents an additional electron from entering. After t_L the pulse amplitude is changed to V_R such that the energy level of the ES is pushed above E_F while the GS level

remains below. Therefore, the charge carrier can only tunnel off the QD if it was loaded onto the ES in the previous phase. Once the charge carrier has left the QD from the ES, the Coulomb blockade is lifted and another charge carrier can tunnel into the GS. The combination of these two processes, tunneling out from the ES, followed by tunneling into the GS, leads to a characteristic "blip" in the detector voltage, indicative of ES loading during the load phase. Note that here we pulse the ES above E_F of the leads, in contrast to the transport measurements before, where we aligned the ES level with the leads during the read phase. After t_R we enter the unload phase, where the pulse amplitude is changed to V_U, and both energy levels are pushed above E_F emptying the QD. As a response to the three-level pulse we expect a change of voltage across the sensing QD consisting of two contributions. First, due to capacitive coupling between PG and the sensing QD the voltage will change proportionally to the applied pulse amplitude. Second, the voltage across the sensing QD traces the charge occupation of the QD, stepping up or down as soon as a charge carrier tunnels off or on the QD. Whenever we load the GS during load phase, the voltage trace should stay flat during t_R. Therefore, measuring whether the voltage trace shows a blip or not during the readout phase forms the basis of our single-shot readout mechanism.

To find the appropriate alignment of the read level for ES-dependent tunneling we sweep V_{PG} while keeping the three-level pulse amplitude constant. We choose pulses with $t_L = 10$ ms, $t_R = 30$ ms, and $t_U = 20$ ms, long enough to allow the charge carrier to tunnel in and out of the QD. The pulse voltages V_L and V_U ensure that both energy levels are pushed below (above) E_F of the leads during the load (unload) phase. Starting with V_{PG} being too low, both the $|\uparrow\rangle$ and the $|\downarrow\rangle$ level lie above E_F, such that the charge carrier can always tunnel off the QD regardless of being in the ES or the GS. The characteristic voltage trace in this regime only shows a step up corresponding to the unloading event, and then remains at this higher level as shown in Fig. 3(d) bottom panel. Increasing V_{PG} we enter the regime of random telegraph signals corresponding to the $|\uparrow\rangle$ level being aligned with E_F of the leads such that a charge carrier can tunnel on and off the QD multiple times within the read phase as observed in Fig. 3(d) middle panel. Increasing V_{PG} further we find the correct read level where we can distinguish between the $|\uparrow\rangle$ and the $|\downarrow\rangle$ state of the QD being occupied. A single blip at the beginning of the read phase corresponds to the ES tunneling off the QD and subsequent tunneling into the GS from one of the leads. A flat trace during t_R indicates that the charge carrier was loaded into the GS during the load phase, and is thus trapped on the QD. Alternatively, the ES could have been loaded relaxing into the GS, before tunneling out. In this region the condition $\mu_{\mathrm{ES}} > E_F > \mu_{\mathrm{GS}}$ is fulfilled and we can perform a single-shot projective measurement of the state of the charge carrier. Exemplary traces for the two cases are shown in Fig. 3(d) top panel, with the blue trace corresponding to the GS and the orange one with the characteristic blip corresponding to the ES.

Averaging the read-phase voltage across the sensing QD $\langle V_{\mathrm{detector}}\rangle$ over 500 single-shot traces at different plunger gate voltages V_{PG} we estimate the probability of the QD being occupied as a function of time shown in Fig. 3(c). The correct readout configuration shows a lower probability in the beginning of the read phase, as observed in the upper part of Fig. 3(c) from $V_{\mathrm{PG}} = -6.3465$ V to $V_{\mathrm{PG}} = -6.3436$ V.

Analyzing a data set consisting of 7500 single-shot measurements we extract the histogram of the peak values of the detector voltage V_{detector} shown in Fig 4(a). We identify two well-separated peaks indicating that V_{Detector} has two favorable values corresponding to the first electron being or not being in the QD. The two voltage levels are separated with a $\mathrm{SNR} = |\mu_1 - \mu_2| / \sqrt{\sigma_1^2 + \sigma_2^2} = 6.95$ as obtained from fitting two skewed Gaussians $A \exp\left[-(x-\mu)^2/2\sigma^2\right][1 - \mathrm{erf}(\gamma(x-\mu)/\sqrt{2}\sigma)]$. This SNR corresponds to an electrical readout fidelity well above 99%. However, the tunneling-out and relaxation rate of the ES are of the same order of magnitude, reducing the fidelity of the spin-to-charge conversion.

Tunneling-out events from the ES can only be observed if the ES does not decay into the GS after tunneling in during the load phase or before tunneling out during the read phase. Thus, varying the length of the load phase gives information about the spin-relaxation time T_1, since the number of observed blips exponentially decays with a longer load phase. As shown in Fig. 4(b), the total number of blips increases for short load times t_L before decreasing exponentially with the characteristic spin-relaxation time scale T_1. For short t_L, the number of observed blips is limited by the overall tunneling rate into either $|\uparrow\rangle$ or $|\downarrow\rangle$. To extract T_1, the function $C(\exp(-t_{\mathrm{L}}/T_1) - \exp(-\Gamma_{\mathrm{in}} t_{\mathrm{L}}))$ is fitted to the data with fitting parameters C and T_1. The parameter $\Gamma_{\mathrm{in}} = 350 \pm 12$ Hz is the total tunneling rate into the QD during the load phase. We find $T_1 = 8.37 \pm 0.34$ ms at $B_\perp = 2.1$ T for the data in Fig. 4(b). As presented in Fig. 4(c), the relaxation time tends to increase with decreasing magnetic field. Data points for the same field configuration are individual measurements where T_1 scatters randomly for different tunnel barrier voltages [see Fig. S1(c) within the Supplemental Material [37]]. While we could not observe a temperature-dependent change of T_1 for 45 mK $< T <$ 120 mK, we find a strong dependence on magnetic field and measure a maximum $T_1 = 50$ ms at $B_\perp = 1.7$ T. Compared to GaAs [25,36], the measured T_1 is large as expected from the lower nuclear spin density and the weaker spin-orbit interactions in graphene [38]. For other group-IV elements, such as silicon, T_1 times between 1 ms and up to 9 s have been reported [30,31].

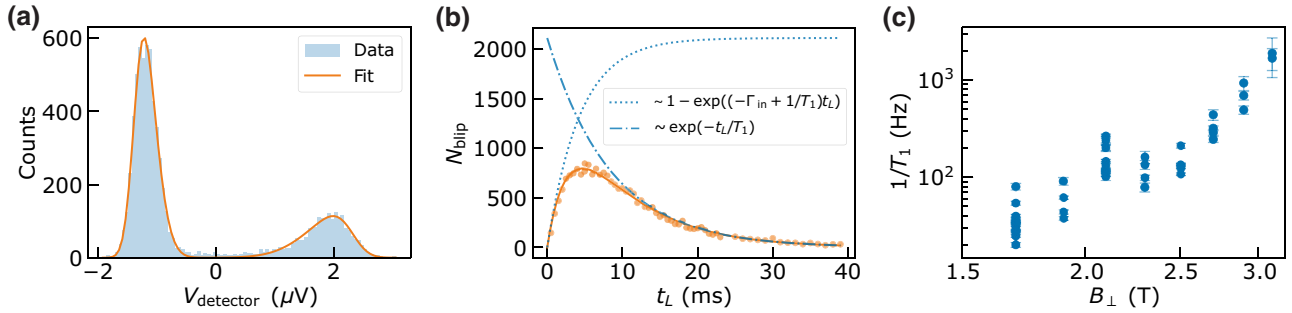

FIG. 4. (a) Histogram of maximum detector voltage values during the read phase. The histogram is fitted with two skewed Gaussians with $\gamma_{GS} = -1.7$, $\mu_{GS} = -1.4$ μV, $\sigma_{GS} = -0.27$ μV and $\gamma_{ES} = 2.76$, $\mu_{ES} = 2.3$ μV, $\sigma_{ES} = -0.6$ μV. (b) Number of blips observed during read phase as a function of loading time. The relaxation time is extracted from the exponential decay. (c) Magnetic field dependence of the relaxation rate $1/T_1$. Data points for one magnetic field correspond to statistically independent measurements.

For bilayer graphene T_1 lies within the same order of magnitude and shows a similar dependence on magnetic field, promising even higher values for smaller Zeeman splitting at lower magnetic field. A sufficient reduction of the tunneling rates for further T_1 measurements at lower magnetic fields cannot be achieved with the current device. Typical mechanisms that determine T_1 are spin-orbit-induced phonon scattering and hyperfine interaction. The limiting mechanism in bilayer graphene remains to be investigated. Nevertheless, we expect similar relaxation times for electrons and holes in bilayer graphene.

IV. CONCLUSION

In conclusion, we first characterized the lifetime of excited states in a graphene QD through direct transport measurements. The measurement is limited by signal strength rather than the relaxation time, comparable to previous measurements performed in bilayer graphene QDs. In a second step we presented a QD device integrated with a capacitively coupled charge sensor capable of resolving a single charge tunneling event in the time domain. The sensitivity of the charge detector enables excited-state readout in the single-shot limit—an essential step towards a fully controllable quantum processor in graphene. We measured spin-relaxation times up to 50 ms at $B_\perp = 1.7$ T, where T_1 strongly depends on the magnetic field applied, promising even longer times for lower fields. The extracted values of T_1 are comparable to the spin-relaxation times in most semiconductor spin qubits, showing that spin qubits in bilayer graphene QDs are promising.

ACKNOWLEDGMENTS

We are grateful for the technical support from Peter Märki, Thomas Bähler, and the staff of the ETH FIRST cleanroom facility. We thank Luca Banszerus and Christian Volk for discussions. We acknowledge financial support by the European Graphene Flagship, the ERC Synergy Grant Quantropy, the European Union's Horizon 2020 research and innovation programme under Grant Agreement No. 862660/QUANTUM E LEAPS and NCCR QSIT (Swiss National Science Foundation, Grant No. 51NF40-185902) and under the Marie Sklodowska-Curie Grant Agreement No. 766025. K.W. and T.T. acknowledge support from the Element Strategy Initiative conducted by the MEXT, Japan, Grant No. JPMXP0112101001, JSPS KAKENHI Grant No. JP20H00354, and the CREST (JPMJCR15F3), JST.

[1] D. Loss and D. P. DiVincenzo, Quantum computation with quantum dots, Phys. Rev. A **57**, 120 (1998).
[2] P. Stano and D. Loss, Review of performance metrics of spin qubits in gated semiconducting nanostructures arXiv:2107.06485 [cond-mat.mes-hall] (2021).
[3] M. Veldhorst, J. C. C. Hwang, C. H. Yang, A. W. Leenstra, B. de Ronde, J. P. Dehollain, J. T. Muhonen, F. E. Hudson, K. M. Itoh, A. Morello, and A. S. Dzurak, An addressable quantum dot qubit with fault-tolerant control-fidelity, Nat. Nanotechnol. **9**, 981 (2014).
[4] C. H. Yang, K. W. Chan, R. Harper, W. Huang, T. Evans, J. C. C. Hwang, B. Hensen, A. Laucht, T. Tanttu, F. E. Hudson, S. T. Flammia, K. M. Itoh, A. Morello, S. D. Bartlett, and A. S. Dzurak, Silicon qubit fidelities approaching incoherent noise limits via pulse engineering, Nat. Electron. **2**, 151 (2019).
[5] M. Veldhorst, C. H. Yang, J. C. C. Hwang, W. Huang, J. P. Dehollain, J. T. Muhonen, S. Simmons, A. Laucht, F. E. Hudson, K. M. Itoh, A. Morello, and A. S. Dzurak, A two-qubit logic gate in silicon, Nature **526**, 410 (2015).
[6] T. Nakajima, A. Noiri, K. Kawasaki, J. Yoneda, P. Stano, S. Amaha, T. Otsuka, K. Takeda, M. R. Delbecq, G. Allison, A. Ludwig, A. D. Wieck, D. Loss, and S. Tarucha, Coherence of a Driven Electron Spin Qubit Actively Decoupled from Quasistatic Noise, Phys. Rev. X **10**, 011060 (2020).
[7] P. Cerfontaine, T. Botzem, D. P. DiVincenzo, and H. Bluhm, High-Fidelity Single-Qubit Gates for Two-Electron Spin Qubits in GaAs, Phys. Rev. Lett. **113**, 150501 (2014).
[8] J. M. Nichol, L. A. Orona, S. P. Harvey, S. Fallahi, G. C. Gardner, M. J. Manfra, and A. Yacoby, High-fidelity

entangling gate for double-quantum-dot spin qubits, Npj Quantum Inf. **3**, 3 (2017).

[9] X. Xue, M. Russ, N. Samkharadze, B. Undseth, A. Sammak, G. Scappucci, and L. M. K. Vandersypen, Computing with spin qubits at the surface code error threshold arXiv:2107.00628 [quant-ph] (2021).

[10] D. M. Zajac, A. J. Sigillito, M. Russ, F. Borjans, J. M. Taylor, G. Burkard, and J. R. Petta, Resonantly driven cnot gate for electron spins, Science **359**, 439 (2018).

[11] J. Yoneda, K. Takeda, T. Otsuka, T. Nakajima, M. R. Delbecq, G. Allison, T. Honda, T. Kodera, S. Oda, and Y. Hoshi *et al.*, A quantum-dot spin qubit with coherence limited by charge noise and fidelity higher than 99.9%, Nat. Nanotechnol. **13**, 102 (2018).

[12] A. R. Mills, C. R. Guinn, M. J. Gullans, A. J. Sigillito, M. M. Feldman, E. Nielsen, and J. R. Petta, Two-qubit silicon quantum processor with operation fidelity exceeding 99% arXiv:2111.11937 [quant-ph] (2021).

[13] N. W. Hendrickx, W. I. L. Lawrie, M. Russ, F. van Riggelen, S. L. de Snoo, R. N. Schouten, A. Sammak, G. Scappucci, and M. Veldhorst, A four-qubit germanium quantum processor, Nature **591**, 580 (2021).

[14] R. Maurand, X. Jehl, D. Kotekar-Patil, A. Corna, H. Bohuslavskyi, R. Laviéville, L. Hutin, S. Barraud, M. Vinet, and M. Sanquer *et al.*, A CMOS silicon spin qubit, Nat. Commun. **7**, 13575 (2016).

[15] L. C. Camenzind, S. Geyer, A. Fuhrer, R. J. Warburton, D. M. Zumbühl, and A. V. Kuhlmann, A spin qubit in a fin field-effect transistor. arXiv:2103.07369 [cond-mat.mes-hall] (2021).

[16] Y. Liu, X. Duan, H.-J. Shin, S. Park, Y. Huang, and X. Duan, Promises and prospects of two-dimensional transistors, Nature **591**, 43 (2021).

[17] C. Tong, R. Garreis, A. Knothe, M. Eich, A. Sacchi, K. Watanabe, T. Taniguchi, V. Fal'ko, T. Ihn, K. Ensslin, and A. Kurzmann, Tunable valley splitting and bipolar operation in graphene quantum dots, Nano Lett. **21**, 1068 (2021).

[18] R. Garreis, A. Knothe, C. Tong, M. Eich, C. Gold, K. Watanabe, T. Taniguchi, V. Fal'ko, T. Ihn, K. Ensslin, and A. Kurzmann, Shell Filling and Trigonal Warping in Graphene Quantum Dots, Phys. Rev. Lett. **126**, 147703 (2021).

[19] S. Möller, L. Banszerus, A. Knothe, C. Steiner, E. Icking, S. Trellenkamp, F. Lentz, K. Watanabe, T. Taniguchi, L. Glazman, V. Fal'ko, C. Volk, and C. Stampfer, Probing two-electron multiplets in bilayer graphene quantum dots. arXiv:2106.08405 [cond-mat.mes-hall] (2021).

[20] A. Kurzmann, Y. Kleeorin, C. Tong, R. Garreis, A. Knothe, M. Eich, C. Mittag, C. Gold, F. K. de Vries, K. Watanabe, T. Taniguchi, V. Fal'ko, Y. Meir, T. Ihn, and K. Ensslin, Kondo effect and spin–orbit coupling in graphene quantum dots, Nat. Commun. **12**, 6004 (2021).

[21] C. Tong, A. Kurzmann, R. Garreis, W. W. Huang, S. Jele, M. Eich, L. Ginzburg, C. Mittag, K. Watanabe, T. Taniguchi, K. Ensslin, and T. Ihn, Pauli blockade of tunable two-electron spin and valley states in graphene quantum dots. arXiv:2106.04722 [cond-mat.mes-hall] (2021).

[22] L. Banszerus, S. Möller, C. Steiner, E. Icking, S. Trellenkamp, F. Lentz, K. Watanabe, T. Taniguchi, C. Volk, and C. Stampfer, Spin-valley coupling in single-electron bilayer graphene quantum dots, Nat. Commun. **12**, 5250 (2021).

[23] A. Kurzmann, H. Overweg, M. Eich, A. Pally, P. Rickhaus, R. Pisoni, Y. Lee, K. Watanabe, T. Taniguchi, T. Ihn, and K. Ensslin, Charge detection in gate-defined bilayer graphene quantum dots, Nano Lett. **19**, 5216 (2019).

[24] T. Fujisawa, Y. Tokura, and Y. Hirayama, Transient current spectroscopy of a quantum dot in the Coulomb blockade regime, Phys. Rev. B **63**, 081304 (2001).

[25] R. Hanson, B. Witkamp, L. M. K. Vandersypen, L. H. W. van Beveren, J. M. Elzerman, and L. P. Kouwenhoven, Zeeman Energy and Spin Relaxation in a One-Electron Quantum Dot, Phys. Rev. Lett. **91**, 196802 (2003).

[26] L. Banszerus, K. Hecker, S. Möller, E. Icking, K. Watanabe, T. Taniguchi, C. Volk, and C. Stampfer, Spin relaxation in a single-electron graphene quantum dot. arXiv:2110.13051 [cond-mat.mes-hall] (2021).

[27] J. M. Elzerman, R. Hanson, L. H. Willems van Beveren, B. Witkamp, L. M. K. Vandersypen, and L. P. Kouwenhoven, Single-shot read-out of an individual electron spin in a quantum dot, Nature **430**, 431 (2004).

[28] F. H. L. Koppens, C. Buizert, K. J. Tielrooij, I. T. Vink, K. C. Nowack, T. Meunier, L. P. Kouwenhoven, and L. M. K. Vandersypen, Driven coherent oscillations of a single electron spin in a quantum dot, Nature **442**, 766 (2006).

[29] N. W. Hendrickx, W. I. L. Lawrie, L. Petit, A. Sammak, G. Scappucci, and M. Veldhorst, A single-hole spin qubit, Nat. Commun. **11**, 3478 (2020).

[30] C. H. Yang, A. Rossi, R. Ruskov, N. S. Lai, F. A. Mohiyaddin, S. Lee, C. Tahan, G. Klimeck, A. Morello, and A. S. Dzurak, Spin-valley lifetimes in a silicon quantum dot with tunable valley splitting, Nat. Commun. **4**, 2069 (2013).

[31] V. N. Ciriano-Tejel, M. A. Fogarty, S. Schaal, L. Hutin, B. Bertrand, L. Ibberson, M. F. Gonzalez-Zalba, J. Li, Y.-M. Niquet, M. Vinet, and J. J. Morton, Spin Readout of a CMOS Quantum Dot by Gate Reflectometry and Spin-Dependent Tunneling, PRX Quantum **2**, 010353 (2021).

[32] A. Knothe and V. Fal'ko, Quartet states in two-electron quantum dots in bilayer graphene, Phys. Rev. B **101**, 235423 (2020).

[33] S. Konschuh, M. Gmitra, D. Kochan, and J. Fabian, Theory of spin-orbit coupling in bilayer graphene, Phys. Rev. B **85**, 115423 (2012).

[34] D. Huertas-Hernando, F. Guinea, and A. Brataas, Spin-orbit coupling in curved graphene, fullerenes, nanotubes, and nanotube caps, Phys. Rev. B **74**, 155426 (2006).

[35] L. Banszerus, K. Hecker, E. Icking, S. Trellenkamp, F. Lentz, D. Neumaier, K. Watanabe, T. Taniguchi, C. Volk, and C. Stampfer, Pulsed-gate spectroscopy of single-electron spin states in bilayer graphene quantum dots, Phys. Rev. B **103**, L081404 (2021).

[36] T. Fujisawa, D. G. Austing, Y. Tokura, Y. Hirayama, and S. Tarucha, Allowed and forbidden transitions in artificial hydrogen and helium atoms, Nature **419**, 278 (2002).

[37] See Supplemental Material at http://link.aps.org/supplemental/10.1103/PRXQuantum.3.020343 for the characterization of the spin excited state as well as the dependence of the spin-relaxation time on the applied barrier voltage.

[38] B. Trauzettel, D. V. Bulaev, D. Loss, and G. Burkard, Spin qubits in graphene quantum dots, Nat. Phys. **3**, 192 (2007).